Targeted Removal of Interfacial Adventitious Carbon towards Directional Charge Delivery to Isolated Metal Sites for Efficient Photocatalytic H_2 Production

Yunxiang Li[a,b], Shengyao Wang[b,e,*], Pei Wang[e], Yu He[b], Xusheng Wang[b], Kun Chang[b], Huiwen Lin[b], Xing Ding[e], Hao Chen[e], Hongwei Zhang[f], Yasuo Izumi[f], Tetsuya Kako[b] and Jinhua Ye[a,b,c,d,*]

[a] Graduate School of Chemical Sciences and Engineering, Hokkaido University, Sapporo 060-0814, Japan

[b] International Center for Materials Nanoarchitectonics (WPI-MANA), National Institute for Materials Science (NIMS), 1-1 Namiki, Tsukuba, Ibaraki 305-0044, Japan

[c] TJU-NIMS International Collaboration Laboratory, School of Materials Science and Engineering, Tianjin University, Tianjin 300072, P. R. China

[d] Collaborative Innovation Center of Chemical Science and Engineering (Tianjin), Tianjin 300072, P. R. China

[e] College of Science, Huazhong Agricultural University, Wuhan, 430070, P. R. China

[f] Department of Chemistry, Graduate School of Science, Chiba University, Yayoi 1-33, Inage-Ku, Chiba 263-8522, Japan

*Corresponding authors.

E-mail addresses: Jinhua.YE@nims.go.jp (J. Ye); wangshengyao@mail.hzau.edu.cn (S. Wang)

Abstract

Creation of clean interfaces without contamination of adventitious carbon and robust single active sites are highly desirable for delivery and utilization of electrons in sunlight-driven hydrogen production but still remains challenging in part owing to the lack of understanding in junction nature. Herein, we tackle this challenge by targeted removing of interfacial adventitious carbon between photoharvester CdS and novel single-cobalt co-catalyst (Co-NC). It's found that surface-trapped electrons can readily migrate to the closely attached Co-NC across the cleared interface between CdS and Co-NC. The small-resistance interfacial carrier path and the robust single-cobalt sites work in a cooperative way and hence achieve a superior visible-light driven H_2 generation activity with a rate of 4.34 mmol/h, an apparent quantum yield (AQY) of 63.9 % at 400 nm and a ultrahigh turnover frequency (TOF) of up to 16714.7 h^{-1}. Our finding will motivate future work in creating clean interfaces and unique single active sites for high performance photocatalysis.

Keywords: interface engineering, cleared interface, adventitious carbon, single-atom catalyst, photocatalytic H_2 generation

1. Introduction

Efficient conversion of renewable solar energy into clean H_2 via photocatalytic water splitting has been widely regarded as an attractive approach to solve the energy crisis and environment problem.[1-3] However, it still remains a great challenge to construct a low cost, robust system for highly efficient photocatalytic H_2 evolution despite enormous progress in this field during the past decades.[4] Most photocatalysts lack active sites on the surface for targeted reactions, leading to the fast recombination of excited carriers and poor performance.[5, 6] Loading co-catalysts with robust active sites can not only lower the activation energy of reactants but also accelerate the electron-hole separation at the semiconductor/co-catalyst interface.[7, 8]

To date, great achievement has been made in exploring noble-metal-free co-catalysts to replace precious metal for constructing efficient photocatalytic system.[9-15] However, several major issues related to the intrinsic properties of current co-catalysts still exist for H_2 generation: (i) low atom utilization efficiency of the metal in co-catalysts because they usually exist as aggregated status; (ii) lack of surface functionalities to form robust connection with semiconductors towards fast transfer of carriers across junction; (iii) unfavorable Gibbs free energy for H_2 generation. Hence, it is highly imperative to design and construct favorable active sites with merits of cost-effective, high utilization efficiency and high turnover frequency for realizing efficient solar energy conversion.

Single-site catalysts, with isolated metal sites supported on solid substrates, especially on N-rich carbon (NC), are emerging as a highly attractive class of catalysts because of their unusual electronic structures, extraordinary catalytic properties, etc.[16-21] These materials feature diverse moieties such as rich N species[22] on surface, tunable metal sites with flexible coordination[23-25] and maximum utilization of metal-site[26] especially when those single

sites are anchored on ultrathin support. These attractive characteristics of single-atom embedded carbon-based family might be utilized for solving the issues mentioned above and render it to be highly promising as co-catalysts. However, such kind of materials have rarely been used as co-catalysts in photocatalytic system, especially for achieving outstanding performance in photocatalysis.

The co-catalysts with elaborate single-site can generate the targeted product upon capturing the energetic photoelectrons; however, it also inevitably brings a contaminated interface between photohavester and co-catalyst caused by the adventitious carbon at the junction. The interfaces, where electrons shuttle, are extremely crucial for efficient photochemistry process. A contaminated interface will severely block the electron transfer to the co-catalytic single-site and such negative effect might also exist for various advanced heterostructures[27-31]. It is worth stressing that surface adventitious carbon widely exists on various materials, such as TiO_2, carbon nitride and black phosphorus;[32-35] upon forming heterostructure, these carbon species will locate at the interface and lead some substantial and underlying effects on the photocatalytic process. However, the detailed roles of those adventitious carbon at the surface or interface in photocatalysis are often neglected but should arise our attention. Recently, Diebold et al. disclosed that TiO_2 selectively adsorbs carboxylic acids on its surface from air/solution and further pointed out the potential effect of the surface carboxylate monolayers on photocatalysis;[32] Medford et al. revealed that the surface adventitious carbon could strongly interact with N_2 molecules and promote photocatalytic N_2 fixation.[33] Further clarifying the exact effect of these carbon species located interfaces in heterostructures are quite essential for constructing robust photocatalytic system but has not been explored at present.

Motivated by the aforementioned key issues, we seek to create a clean heterostructured interface aiming at speeding up the carriers flow to the robust single-site co-catalysts for constructing photocatalytic system with record activity and metal utilization efficiency. Herein, we report a rational design and novel synthesis of single Co implanted ultrathin N-rich carbon

nanosheets (Co-NC) and create a cleared junction between photoharvester CdS and co-catalyst Co-NC through calcination-induced elimination of interfacial adventitious carbon. The cleared interfaces collaborate with the robust isolated Co-N_4 sites to achieve an outstanding visible-light-driven H_2 evolution activity with a rate of 4.34 mmol/h, an AQY of 63.9% at 400 nm. Remarkably, the optimal system achieves an ultrahigh TOF_{Co} of up to 16714.7 h^{-1}. This new strategy constructs an efficient system for H_2 photogeneration via creating robust single-atom co-catalyst Co-NC and simultaneously clearing the interface between CdS and Co-NC. This built-in system not only clarifies the significant blocking effect of widely existed surface adventitious carbon on charge transport, but also highlights both the essential roles of cleared interface and single-atom based materials in photocatalysis.

2. Experimental section

2.1 Sample preparation

Synthesis of (M)-NC: Co/Zn-supermolecular precursor was first prepared by a facile and scalable wet-chemical method. Typically, melamine (1.26g, 10 mmol), $Zn(OAc)_2$ (1.82g, 9.9 mmol) and $Co(OAc)_2 \cdot 4H_2O$ (24.91 mg, 0.1 mmol) was added to 100 mL methanol with vigorous stirring, then the dispersion was transferred to an oil bath and refluxed at 70 ^oC for 3 h. The obtained light pink solid was centrifuged and washed with ethanol for two times, then dried at 70 ^oC under vacuum. The yield wad estimated to be 85.8 % with 2.66 g light pink powder product.

Subsequently, the above powder precursor underwent a two-stage pyrolysis and carbonization process (retained at 650 ^oC for 1h, then increased to at 950 ^oC and held for 3 h with a ramping rate of 3 ^oC/min) in tube furnace under argon atmosphere. After cooling down to the room temperature, the obtained black product was leached with 0.5 M HCl to remove metal particles and unstable species and successively washed using distilled water. Afterwards, the obtained sample was further crushed into small-sized ultrathin nanosheets by ball milling treatment, the final resultant sample was denoted as Co-NC. A typical wet-milling was performed on a

planetary ball mill (Fritsch, P-7) and conducted at 400 rpm for 15 h using distilled water as the solvents.

Other (M)-NC(NS) (M = Fe, Ni) were synthesized using similar procedure, except employing different metal precursors and different solvents for the preparation of corresponding supermolecular precursors. In detail, 0.1 mmol $Fe(NO_3)_3 \cdot 9H_2O$ and 0.1 mmol $NiCl_2 \cdot 6H_2O$ severed as the metal source for precursor fabrication of Fe-NC and Ni-NC. In the case of Ni-NC, 10 mL ethanol and 90 mL methanol was employed as the solvent to prepare the precursor. For NC, only 10 mmol $Zn(OAc)_2$ was used to prepare the precursor.

Preparation of CdS/Co-NC composites: well-dispersed (M)-NC in aqueous solution was added into the dispersion of commercial CdS with stirring, after stirring for 5 mins, the mixture was filtered and dried at 30 ^oC under vacuum. A series of CdS/Co-NC samples with different Co-NC content (0.5, 1, 1.5, 2.0, 2.5 wt %) were prepared. To reinforce the interface interaction between CdS and (M)-NC, the dried sample was annealed at different temperature (400, 450, 500, 550 ^oC) for 1 h under Ar atmosphere. The CdS/Co-NC(RT) and CdS/Co-NC(500) refers to the hybrid CdS/Co-NC without and with annealing at 500 ^oC under Ar atmosphere, respectively. The composites with different loading amount or treated at different temperature will be specifically stated.

2.2 Material characterization: XRD patterns of the as-prepared samples were collected with a powder X-ray diffractometer (Cu Kα radiation source, X'pert powder, PANalytical B.V., Netherlands). UV−visible (UV−vis) diffuse reflectance spectra of the samples were recorded on an UV−visible spectrophotometer (UV-2700, Shimadzu, Japan) equipped with an integrating sphere, then converted into absorption spectra by Kubelka−Munk transformation. Nitrogen adsorption–desorption isotherms, and surface area were recorded using a BEL SORP-mini II (BEL Japan INC., Japan), and were calculated via the Brunauer-Emmett-Teller (BET) method. The Photoluminescence (PL) properties were investigated using a fluorescence spectrophotometer (Fluorolog-3, HORIBA Scientific, America). X-ray photoelectron

spectroscopy (XPS) measurements were carried out on XPS instrument (Escalab 250, Thermo SCIENTIFIC, America). All binding energies were referenced to the C *1s* peaks of the surface adventitious carbon at 284.8 eV. The morphologies of samples were characterized with Field Emission Scanning Electron Microscope (JSM-6701F, JEOL Co., Japan) and Transmission Electron Microscope (TEM) (JEM-2100F, JEOL Co., Japan). Energy-dispersive X-ray spectroscopy (EDS) mapping was also recorded with same TEM instrument. The STEM characterizations were performed on a JEOL ARM-200F field-emission transmission electron microscope. Raman spectra were collected using a Horiba Jobin Yvon LabRAM system with a 532 nm excitation laser. The electron spin resonance (ESR) measurements were performed on an ESR spectrometer (JES-FA200, JEOL Co., Japan) at liquid nitrogen temperature (77 K). The X-ray absorption fine structure spectra were performed at 1W1B station in Beijing Synchrotron Radiation Facility (BSRF). The XAFS data were recorded in fluorescence excitation mode using a Lytle detector. Co foil, CoO and Co_3O_4 were used as the reference. The acquired XAFS data were analyzed by Athena and Artemis interfaces to the IFFEFIT software, according to the standard procedures.

2.3 Photocatalytic activity evaluation: The photocatalytic H_2 evolution test was carried out in a glass reactor with a closed gas circulation system. In a typical test, 150 mg photocatalyst was firstly dispersed with a magnetic stirrer in 280 mL 20 vol % lactic acid solution (the pH of the solution was adjusted by NaOH in advance). After vacuumizing, H_2 evolution over the photocatalyst was carried out under visible light irradiation (light source, 300 W Xe lamp equipped with an L42 cutoff filter, $\lambda > 400$ nm). The evolved H_2 was analyzed by online gas chromatography (GC-8A; Shimadzu Corp., Japan) equipped with a thermal conductivity detector. The photocatalytic H_2 generation rates over as-prepared samples was fitted with the four points ranging from 0.5 h to 2h.

The apparent quantum efficiency (AQY) was measured under similar conditions as described above except for the light intensity and the wavelength regions of the irradiation light. A series of band-pass filters were adopted to control the wavelength regions of incident light. A water filer was also used together with the band-pass filter to avoid the possible damage caused by heating effect of Xe lamp. The average intensity of irradiation was determined by using a spectroradiometer (Ushio, USR-40, Japan). The AQY at each monochromatic wavelength was calculated by following the equation below:

AQY for H_2 evolution = N(H_2) * 2 / N(photons) * 100%

Note: N(H_2) represents the molecular number of evolved H_2 and N(photons) means the number of incident photons.

3. Results and discussion

3.1 Synthesis and characterization of co-catalyst Co-NC

The ultrathin single atom co-catalysts ((M)-NC; M = Co, Fe, Ni) were synthesized mainly via two steps as illustrated in Figure 1a: (i) pyrolysis of a supramolecular precursor; (ii) downsizing the obtained hierarchical sheets into small-sized ultrathin nanosheets by ball milling treatment. X-ray powder diffraction (XRD) pattern of Co-NC (Figure S1a) exhibits a broad peak centered at ~26.0º, assigned to the (002) plane of graphitic carbon. Raman spectra (Figure S1b) show two typical signals belonging to defect-rich carbon, i.e., D band (1355.9 cm^{-1}) and G band at (1591.6 cm^{-1}). The Co-NC possesses a specific surface area of 222.7 m^2/g (Figure S2) and presents as uniform 2D sheets with a planar size of ~200 nm (Figure 1b and Figure S3) and an ultrathin thickness of ~1.5 nm (Figure S4). The high-resolution transmission electron microscopy (HRTEM) image (Figure 1c) reveals some typical fringes, corresponding to few-layer carbon sheet. In particular, no signal of Co clusters or nanoparticles are detected on the ultrathin nanosheets by scanning electron microscopy (SEM), TEM and XRD. The TEM-EDS (energy disperse X-ray) mapping results (Figure 1d) reveal that Co, N and C distribute homogeneously across the entire architecture. Moreover, atomic-resolution aberration-

corrected high-angle dark-field scanning TEM (HAADF-STEM) was used to directly distinguish the Co species with atomic scale. As clearly revealed in Figure 1e, isolated Co sites, appeared as individual bright spots with an average size ~0.2 nm, are well dispersed on the N-rich carbon nanosheets.

The chemical composition and valence states of Co-NC were examined using X-ray photoelectron spectroscopy (XPS) (Figure S5) measurement. The isolated Co sites exhibit a peak at 780.6 eV, corresponding to the Co-N species (Figure S5a).[36] The atomic content of Co in Co-NC determined by XPS is 0.77 at % (3.5 wt %, close to 3.4 wt % examined by inductively coupled plasma atomic emission spectroscopy). Four types of N species (Figure S5b) including pyridinic-N (398.8 eV), pyrrolic-N (400.0 ev), graphitic-N (401.3 eV), oxidized-N (402.8 eV) can be clearly distinguished, among which the pyridinic N serves as the anchor sites for stabilizing the single Co. This assumption was supported by the shift of pyridinic N peak towards higher binding energy after introducing Co species while other kinds of N species remain almost unchanged, revealing the binding formation between Co and pyridinic N.

To further examine the coordination configuration and chemical state of the single Co sites, X-ray absorption fine structure (XAFS) measurements were performed. The results reveal that the Co species exist in an isolated state and stabilized by nitrogen in the form of $Co\text{-}N_4$. Figure 2a presents the X-ray absorption near-edge structure (XANES) spectra of Co-NC in comparison to standard spectra of Co foil, CoO and Co_3O_4. The absorption edge of Co-NC locates between those for CoO and Co_3O_4, and close to that of CoO, clearly suggesting the Co sites deliver a slightly higher oxidation state than Co^{2+}. More detailed structural information of Co sites can be obtained based on extended X-ray absorption fine structure (EXAFS) analysis (Figure 2b). The Co-NC shows a dominant Co-N peak at 1.42 Å, which is shorter than Co-O signal at 1.71 Å in CoO and 1.49 Å in Co_3O_4. Additionally, no Co-Co peak can be observed at 2.12 Å for Co-NC, corroborating the atomic dispersion of single Co sites in Co-NC. We further investigate the coordination of Co sites by EXAFS curve fitting analysis. The surrounded N number of Co

center is estimated to be four according to the fitting results (Table S1). In further electron spin resonance (ESR) analysis (Figure 2d), the similar spectra with close g value for Co-NC and commercial cobalt (II) phthalocyanine (CoPc) at 77 K reveal that the Co sites in Co-NC exhibits similar coordination with four N sites and valence state (Co^{2+}) with those in CoPc, which coincides well with the XAFS analyses (Figure 2a,b,c). Note that the signal pointed by an arrow with the g value of 2.2097 is attributed to the low spin Co (II) in CoPc.[37]

3.2 CdS/Co-NC(500) is about 289 times more active than bare CdS

As single Co sites based catalysts have been reported as promising electrocatalysts for hydrogen evolution,[38] enlightened by this, here we constructed a system composed of CdS/(M)-NC for visible-light-driven hydrogen generation, wherein the CdS serves as the photo-harvester and (M)-NC acts as the co-catalysts for water reduction. The CdS/(M)-NC(RT) and CdS/(M)-NC(500) represent the composites without and with annealing treatments, respectively; the loading amount of co-catalysts for these hybrids is 1 wt% unless otherwise stated. These ultrathin (M)-NC co-catalysts can be uniformly and facilely grafted on the surface of CdS via simple mixing process as identified by the SEM analyses, UV-vis spectra, and TEM elemental mapping analyses (Figure S6, S7 and S8). As shown in Figure 3a, bare CdS shows a poor photocatalytic hydrogen evolution activity of ~15 μmol/h and sole Co-NC is inactive for hydrogen evolution. Remarkably, the coupling of Co-NC with CdS drastically boost the activity of CdS, reaching up to 4.34 mmol/h under optimized conditions (Figure S9) and achieve an apparent quantum yield (AQY) of 63.9% at 400 nm (Figure 3b), representing the currently achieved state-of-the-art H_2 generation activity among all the CdS-based H_2 generation system (Table S2). Such an activity of CdS/Co-NC(500) even far exceeds that of CdS/1wt%Pt under appropriate conditions (Figure 3a). Besides that, the isolated Co sites in this system can afford an ultrahigh turnover frequency (TOF) reaching up to 16714.7 h^{-1} (the number of moles of generated H_2 divided by the number of moles of Co (derived from XPS) in Co-NC) when we altered amount of catalysts (Figure 3c). Such a high TOF value far surpasses that of advanced

Co-based species on CdS (600 h^{-1}) by a factor of 27.9 times.[12] In addition, the CdS/Co-NC(500) exhibits considerable stability as identified by the relatively stable H_2 generation in the four-cycle test (Figure S10a,b; at pH = 6 and 7). Figure 3d shows that the optimal sample CdS/Co-NC(500) can even exhibit an activity of 814 μmol/h with excellent stability under the irradiation of simulated sunlight with a light intensity of 100 mW cm^{-2}. To further judge the advantage of ultrathin morphology of support in H_2 evolution activity, another single-Co (Co-N_4) co-catalysts with rhombic dodecahedron morphology (Co-NC_{rd}) was fabricated according to the previous report[24] (Figure S11 and Figure S12) and further anchored on CdS (Figure S13) followed by heat treatment at 500 °C. Under the same conditions, the CdS with ultrathin Co-NC (Figure S14; 4.34 mmol/h; 4801.7 h^{-1}) achieves a ~3 times H_2 evolution rate and a ~2 times TOF those of CdS/Co-NC_{rd}(500) (1.51 mmol/h; 2249.6 h^{-1}), respectively.

3.3 Cleared interfaces and robust Co-N_4 moieties for high performance

We further explored the reason that the CdS/Co-NC(500) delivers superior photocatalytic hydrogen evolution efficiency. Generally, to fully exploit the activity of a photocatalytic system, three requirements should be met: (i) excellent photohavester with suitable band level and band gap; (ii) high mobility of light-induced carriers from the photoabsorber to active centers; (iii) outstanding active sites to collect the photoelectrons and subsequently transform the reactants into the products. To clarify the exact role of Co-NC in the highly efficient H_2 generation system CdS/Co-NC(500), a contrast experiment was conducted. Besides co-catalyst NC, we also prepared co-catalysts Fe-NC and Ni-NC with isolated Fe and Ni centers (Figure S15) respectively, in a similar way to fabrication of Co-NC. As illustrated in Figure 3e, the co-catalysts NC, Fe-NC and Ni-NC loaded CdS exhibit poor and similar activity of ~1.0 mmol/h, which are much lower than that of Co-NC modified one. Apparently, the isolated Co center in Co-NC with unique properties mainly acts as the active site for superior H_2 evolution. The slight deactivation of CdS/Co-NC(500) at pH = 5 compared with the excellent stability at pH = 7 (Figure S10) lends further support to the essential role of isolated Co sites in H_2 generation. The

acid solution (pH = 5) might slightly etch CdS and generate some free S^{2-} species, which could poison the single Co sites and account for the slight decrease in activity. The stable performance of CdS/NC(500) without discrete Co sites (Figure S16) at pH = 5 further verifies above assumption. Moreover, the annealing process are also quite significant for boosting the performance of CdS/NC and CdS/Co-NC. For both co-catalysts NC and Co-NC, a dramatic enhancement can be observed (Figure 3f) when heat treatment was adopted. Note: annealing process causes no changes on CdS phase as revealed by XRD patterns (Figure S17). The annealing treatment may strengthen the interface interaction between CdS and the attached co-catalysts and thus accelerate the charge transfer from CdS to co-catalysts. In brief, the efficient H_2 evolution activity attributes to both the distinct single Co sites and the potential interface structure evolution caused by annealing considering above contrast experiments. Therefore, we try to gain deeper insight into the underlying mechanism from these two aspects.

First, to unravel the root of the excellent co-catalytic H_2 production performance of Co-N_4 sites embedded in co-catalyst Co-NC, the hydrogen adsorption free energy change ΔG_H on various sites including graphitic-C, graphitic-N, pyridinic-N and metal sites coordinated with four pyridinic-N (the models for calculation are provided in Table S3,4 and Figure S18,19,20), were employed as a descriptor to reflect hydrogen evolution activity. Usually, the ideal value of ΔG_H is 0 eV, which means hydrogen is bound neither too strongly nor too weakly and thus favors both the hydrogen adsorption and consequent desorption. The diagram in Figure 4a demonstrates the isolated Co sites bonded with four N atoms exhibit the nearest value to 0 eV compared with Fe, Co sites with identical coordination environment and other possible sites. This result indicates that the isolated Co sites are the most favorable sites for H_2 evolution among all the studied sites and mainly account for the H_2 generation for CdS/Co-NC(500).

Furthermore, the giant H_2 evolution activity enhancement by the annealing process ignited our interest in disclosing how the interfacial structure evolve upon annealing and how it affects the charge flow across the junction between CdS and Co-NC. A series of characterizations

including HRTEM, XPS, photoelectrochemical method, in situ FT-IR (Fourier transform infrared spectroscopy) and photoluminescence (PL) spectroscopy were adopted to approach the detailed charge flow process and interfacial structure evolution. High-resolution TEM image (Figure 4b) of CdS/Co-NC reveals an intimate interfacial heterostructure composed of ultrathin Co-NC tightly wrapping on a bulk CdS. Such a compact contact between CdS and ultrathin Co-NC could enable the fast electron transfer through the interface. The analyses of chemical valence of Cd, S, C and N contained in the composites allow us to understand the flow direction of electrons. High-resolution Cd *3d* (Figure 4c) and S *2p* XPS spectra (Figure S21) show that both the binding energy of Cd and S increases after loading Co-NC, clearly suggesting the electron donating feature of CdS and thus the electron accepting nature of the Co-NC in CdS/Co-NC obtained without annealing. More interestingly, heat treatment at 500 ^{o}C under Ar can further promote charge flow from CdS to Co-NC as evidenced by the larger binding energy of Cd and S in CdS/Co-NC after annealing, and cause dramatically enhanced H_2 generation activity from ~1.0 to 4.3 mmol/h (Figure 3f). In relative to the NC, the Co-NC possesses stronger ability for collecting the electron from photohavester CdS as identified by the higher binding energy of Cd and S for CdS/Co-NC compared to CdS/NC (Figure 4c and Figure S21). Additionally, the anchored co-catalysts Co-NC, as the electrons acceptor, should present as an electron rich state. The high-resolution N *1s* spectra reveal (Figure 4d) that all N species including pyridinic N coordinated with Co sites, pyrrolic N and graphitic N in Co-NC could accept the donated electron from CdS as verified by the shifted binding energy towards low energy side. Beyond that, the further increased binding energy of pyridinic N sites bonded with Co centers caused by annealing process clearly indicates that the heat treatment can further enrich the electrons on these N sites and then transfer to the active Co sites for H_2 generation. Unfortunately, the content of Co in the composite CdS/Co-NC(500) is too low to detect using XPS method (Figure S22), thus it's difficult to directly observe the electron-rich state of Co sites currently. However, according to the remarkably enhanced activity induced by Co-NC

(Figure 3e) in relative to NC, Fe-NC and Ni-NC, it's rational to conclude that the Co sites can accept the electrons for robust H_2 evolution.

To explore the origin of aforementioned annealing-promoted electrons transfer from CdS to Co-NC and visualize the interfacial structure evolution in the system CdS/Co-NC with annealing, in-situ FT-IR was conducted under elevated temperature and Ar atmosphere, in which CdS/Co-NC(RT) was examined and the detected signal at 100 ^{o}C was used as the background. It's worth noting that surfaces of commercial CdS in our case are covered with abundant adventitious carbon species (Figure S23), similar to the widely studied TiO_{2}[32] and carbon nitride[35]; upon forming heterostructures, the interfaces will be enriched with these carbon species. The calcination-time dependent infrared spectra (Figure 4e) of CdS/Co-NC(RT) present gradually decreased absorbance at ~1000 (O-H, out-of-plane bend), ~1177-1232 (C-O, stretch), ~1405 (C-H, bend), and ~1626 cm^{-1} (C=O, stretch) with increasing temperature, clearly indicating the decomposition of the adventitious carbon. The distinct signals of contrast samples CdS and Co-NC compared with hybrid CdS/Co-NC(RT) indicates that, in CdS/Co-NC(RT), most of those reduced C=O, C-O and OH groups originate from the decomposition of adventitious hydrocarbon confined at the interfaces between CdS and Co-NC rather than on the naked surfaces of CdS and Co-NC (Figure S24 and relevant discussions). Therefore, the fully calcined sample CdS/Co-NC(500) should contain no or very limited interfacial adventitious carbon, which is evidenced by the in-situ FT-IR spectra of fully annealed CdS/Co-NC(500) (Figure S25 and relevant discussions). In brief, annealing process can effectively remove the interfacial adventitious carbon for CdS/Co-NC(RT), which is further supported by the declined C and O content in the calcined CdS/Co-NC(500) detected with XPS method (Figure S26). As a result, a much cleaner interface is created, which could enable the smoother electron transport from CdS to Co-NC. Interestingly, an extra peak appears in high resolution N *1s* spectrum for annealed CdS/Co-NC(500) (Figure 4d) in contrast to CdS/Co-NC obtained at room temperature. This additional signal may come from the N-S bonds at the interfaces between CdS and Co-NC

because of the elimination of interfacial adventitious hydrocarbon after heat treatment. Such an extra bond might act as a new interfacial electron shuttle channel to mediate the electron transfer from CdS to Co-NC. Benefitting from the cleaner junction and the possible newly formed bonds between CdS and Co-NC induced by the increased annealing temperature, the activity of CdS/Co-NC was improved progressively (Figure S9a), which further corroborates the effective annealing-induced clearing of the junction between CdS and Co-NC.

The cleared interfaces enable the fast charge transfer from CdS to Co-NC as identified by in situ FT-IR and XPS analyses. We further focus on the promoted kinetics of photocarriers benefitted from this point by comparing a group of CdS-based composites. Steady-state photoluminescence (PL) spectroscopy characterization, as a powerful tool to monitor the excitonic processes, i.e., radiative recombination of photogenerated electron-hole pairs in photocatalyst, was carried out for a series of samples. As shown in Figure 4f, pristine CdS presents two distinct emission peaks in the range of 385-503 nm and 503-670 nm, assigned to the excitonic emission of CdS and surface states related carriers recombination, respectively.[39] Upon loading Co-NC on CdS without further annealing, the PL peak centered at ~547 nm is substantially suppressed meanwhile the one centered at ~417 nm remains almost unchanged. It signifies that the Co-NC can collect the energetic electrons trapped by surface defect level of CdS although adventitious carbon layer exists between CdS and Co-NC (Scheme 1a). After removing the organic layer by annealing the composite at 500 ^{o}C, Co-NC captures most photogenerated electrons from CdS side as evidenced by the further quenched emission peak in the range of 503-670 nm (Scheme 1b). Consequently, those massively collected electrons will power the robust isolated Co sites for highly efficient hydrogen evolution. Additionally, compared with pristine CdS and CdS/Co-NC(RT) without heating, the obvious blue shift of emission peak related to surface states for annealed CdS/Co-NC(500) could be ascribed to the strong interfacial interaction after eliminating the adventitious carbon at the junctions.

Photoelectrochemical characterizations lend further support to the essential role of smooth

carrier transport channel created by removing the interfacial adventitious carbon. Nyquist plot of CdS/Co-NC(500) under irradiation presents smallest semicircle in comparison with that of the pristine CdS and CdS/Co-NC(RT) (Figure S27a), indicating the smallest resistance across the interface between CdS and Co-NC for annealed CdS/Co-NC(500). Meanwhile, a marked boosted photocurrent (Figure S27b), benefitting from the smoother junction, is also observed for CdS/Co-NC(500) compared to that of CdS and CdS/Co-NC(RT).

According to the analyses above, the outstanding photocatalytic performance of CdS/Co-NC system originates from two reasons: (i) the distinctive single Co sites with moderate attraction for robust H_2 generation; (ii) the smooth carrier channel created by eliminating the interfacial adventitious carbon species between CdS and Co-NC as illustrated in Scheme 1.

4. Conclusions

In summary, our study demonstrates an outstanding visible-light-driven H_2 evolution system CdS/Co-NC(500), which achieves a superb performance with an activity of 4.34 mmol/h, an AQY 63.9% at 400 nm and an remarkably high TOF_{Co} of up to 16714.7 h^{-1}. The excellent performance mainly attributes to two reasons as disclosed by experiment analyses and theoretical investigation. First, eliminating the interfacial adventitious hydrocarbon layer by annealing process enables directional and fast delivery of electron from CdS to Co-NC; second, the isolated Co site coordinated with four N owns favorable hydrogen adsorption ability and thus can fully utilize the collected electrons from photosensitizer for H_2 evolution. This study clarifies the significant negative role of widely existed surface adventitious carbon on materials in photocatalytic process and highlights both the great potential of cleared interface and single-atom based materials in photocatalysis. Thus, our results offer new opportunities for the exploration and design of high-performance system for efficient solar energy-driven conversion.

Acknowledgement

This work received financial support from the World Premier International Research Center Initiative (WPI Initiative) on Materials Nanoarchitectonics (MANA), MEXT (Japan), JSPS KAKENHI (JP18H02065), the Photo-excitonix Project at Hokkaido University, National Natural Science Foundation of China (21633004), Fundamental Research Funds for the Central Universities (No. NE2019103). Y. L. thank Dr. Shuxin Ouyang for his great support as always. The authors are grateful to Beijing Synchrotron Radiation Facilities staff for beam time and for their technical assistance in XAS test.

Declaration of interests

The authors declare no competing financial interests.

References

[1] T.A. Kandiel, I. Ivanova, D.W. Bahnemann, Energy Environ. Sci., 7 (2014) 1420-1425.

[2] H. Tong, S. Ouyang, Y. Bi, N. Umezawa, M. Oshikiri, J. Ye, Adv. Mater., 24 (2012) 229-251.

[3] X. Chen, S. Shen, L. Guo, S.S. Mao, Chem. Rev., 110 (2010) 6503-6570.

[4] A. Kudo, Y. Miseki, Chem. Soc. Rev., 38 (2009) 253-278.

[5] K. Chang, X. Hai, J. Ye, Adv. Energy Mater., 6 (2016) 1502555.

[6] X. Li, J. Yu, M. Jaroniec, X. Chen, Chem. Rev., 119 (2019) 3962-4179.

[7] J. Ran, J. Zhang, J. Yu, M. Jaroniec, S.Z. Qiao, Chem. Soc. Rev., 43 (2014) 7787-7812.

[8] S. Wang, Y. Wang, S.L. Zhang, S.Q. Zang, X.W.D. Lou, Adv. Mater., 31 (2019) e1903404.

[9] J. Ran, G. Gao, F.T. Li, T.Y. Ma, A. Du, S.Z. Qiao, Nat. Commun., 8 (2017) 13907.

[10] J. Li, G. Zhan, Y. Yu, L. Zhang, Nat. Commun., 7 (2016) 11480.

[11] C. Peng, P. Wei, X. Li, Y. Liu, Y. Cao, H. Wang, H. Yu, F. Peng, L. Zhang, B. Zhang, K. Lv, Nano Energy, 53 (2018) 97-107.

[12] G. Zhao, Y. Sun, W. Zhou, X. Wang, K. Chang, G. Liu, H. Liu, T. Kako, J. Ye, Adv. Mater., 29 (2017) 1703258.

[13] H. Zhang, P. Zhang, M. Qiu, J. Dong, Y. Zhang, X.W.D. Lou, Adv. Mater., 31 (2019) e1804883.

[14] Q. Li, B. Guo, J. Yu, J. Ran, B. Zhang, H. Yan, J.R. Gong, J. Am. Chem. Soc., 133 (2011) 10878-10884.

[15] X. Hai, W. Zhou, S. Wang, H. Pang, K. Chang, F. Ichihara, J. Ye, Nano Energy, 39 (2017) 409-417.

[16] Y. Chen, S. Ji, C. Chen, Q. Peng, D. Wang, Y. Li, Joule, 2 (2018) 1242-1264.

[17] C. Gao, S. Chen, Y. Wang, J. Wang, X. Zheng, J. Zhu, L. Song, W. Zhang, Y. Xiong, Adv. Mater., 30 (2018) e1704624.

[18] P. Yin, T. Yao, Y. Wu, L. Zheng, Y. Lin, W. Liu, H. Ju, J. Zhu, X. Hong, Z. Deng, G. Zhou, S. Wei, Y. Li, Angew. Chem. Int. Ed. Engl., 55 (2016) 10800-10805.

[19] J. Wang, Z. Li, Y. Wu, Y. Li, Adv. Mater., 30 (2018) e1801649.

[20] X. Li, X. Yang, Y. Huang, T. Zhang, B. Liu, Adv. Mater., (2019) e1902031.

[21] X. Cui, H. Li, Y. Wang, Y. Hu, L. Hua, H. Li, X. Han, Q. Liu, F. Yang, L. He, X. Chen, Q. Li, J. Xiao, D. Deng, X. Bao, Chem, 4 (2018) 1902-1910.

[22] W. Liu, L. Zhang, X. Liu, X. Liu, X. Yang, S. Miao, W. Wang, A. Wang, T. Zhang, J. Am. Chem. Soc., 139 (2017) 10790-10798.

[23] S. Tian, Q. Fu, W. Chen, Q. Feng, Z. Chen, J. Zhang, W.C. Cheong, R. Yu, L. Gu, J. Dong, J. Luo, C. Chen, Q. Peng, C. Draxl, D. Wang, Y. Li, Nat. Commun., 9 (2018) 2353.

[24] X. Wang, Z. Chen, X. Zhao, T. Yao, W. Chen, R. You, C. Zhao, G. Wu, J. Wang, W. Huang, J. Yang, X. Hong, S. Wei, Y. Wu, Y. Li, Angew. Chem. Int. Ed. Engl., 57 (2018) 1944-1948.

[25] Z. Liang, W. Guo, R. Zhao, T. Qiu, H. Tabassum, R. Zou, Nano Energy, 64 (2019) 103917.

[26] Y. Zhu, W. Sun, J. Luo, W. Chen, T. Cao, L. Zheng, J. Dong, J. Zhang, M. Zhang, Y. Han, C. Chen, Q. Peng, D. Wang, Y. Li, Nat. Commun., 9 (2018) 3861.

[27] J. Low, B. Dai, T. Tong, C. Jiang, J. Yu, Adv. Mater., 31 (2019) 1802981.

[28] J. Ran, W. Guo, H. Wang, B. Zhu, J. Yu, S.Z. Qiao, Adv. Mater., 30 (2018) e1800128.

[29] J. Low, J. Yu, M. Jaroniec, S. Wageh, A.A. Al-Ghamdi, Adv. Mater., 29 (2017) 1601694.

[30] S. Wang, B.Y. Guan, X. Wang, X.W.D. Lou, J. Am. Chem. Soc., 140 (2018) 15145-15148.

[31] S. Wang, B.Y. Guan, X.W.D. Lou, J. Am. Chem. Soc., 140 (2018) 5037-5040.

[32] J. Balajka, M.A. Hines, W.J.I. DeBenedetti, M. Komora, J. Pavelec, M. Schmid, U. Diebold, Science, 361 (2018) 786-789.

[33] B.M. Comer, Y.H. Liu, M.B. Dixit, K.B. Hatzell, Y. Ye, E.J. Crumlin, M.C. Hatzell, A.J. Medford, J. Am. Chem. Soc., 140 (2018) 15157-15160.

[34] S.K. Muduli, E. Varrla, Y. Xu, S.A. Kulkarni, A. Katre, S. Chakraborty, S. Chen, T.C. Sum, R. Xu, N. Mathews, J. Mater. Chem. A, 5 (2017) 24874-24879.

[35] P. Niu, L. Zhang, G. Liu, H.-M. Cheng, Adv. Funct. Mater., 22 (2012) 4763-4770.

[36] Y. Pan, R. Lin, Y. Chen, S. Liu, W. Zhu, X. Cao, W. Chen, K. Wu, W.C. Cheong, Y. Wang, L. Zheng, J. Luo, Y. Lin, Y. Liu, C. Liu, J. Li, Q. Lu, X. Chen, D. Wang, Q. Peng, C. Chen, Y. Li, J. Am. Chem. Soc., 140 (2018) 4218-4221.

[37] A. Singh, S. Roy, C. Das, D. Samanta, T.K. Maji, Chem. Commun. (Camb.), 54 (2018) 4465-4468.

[38] H. Fei, J. Dong, M.J. Arellano-Jimenez, G. Ye, N. Dong Kim, E.L. Samuel, Z. Peng, Z. Zhu, F. Qin, J. Bao, M.J. Yacaman, P.M. Ajayan, D. Chen, J.M. Tour, Nat. Commun., 6 (2015) 8668.

[39] J. Su, T. Zhang, Y. Li, Y. Chen, M. Liu, Molecules, 21 (2016) 735.

Figures and schemes

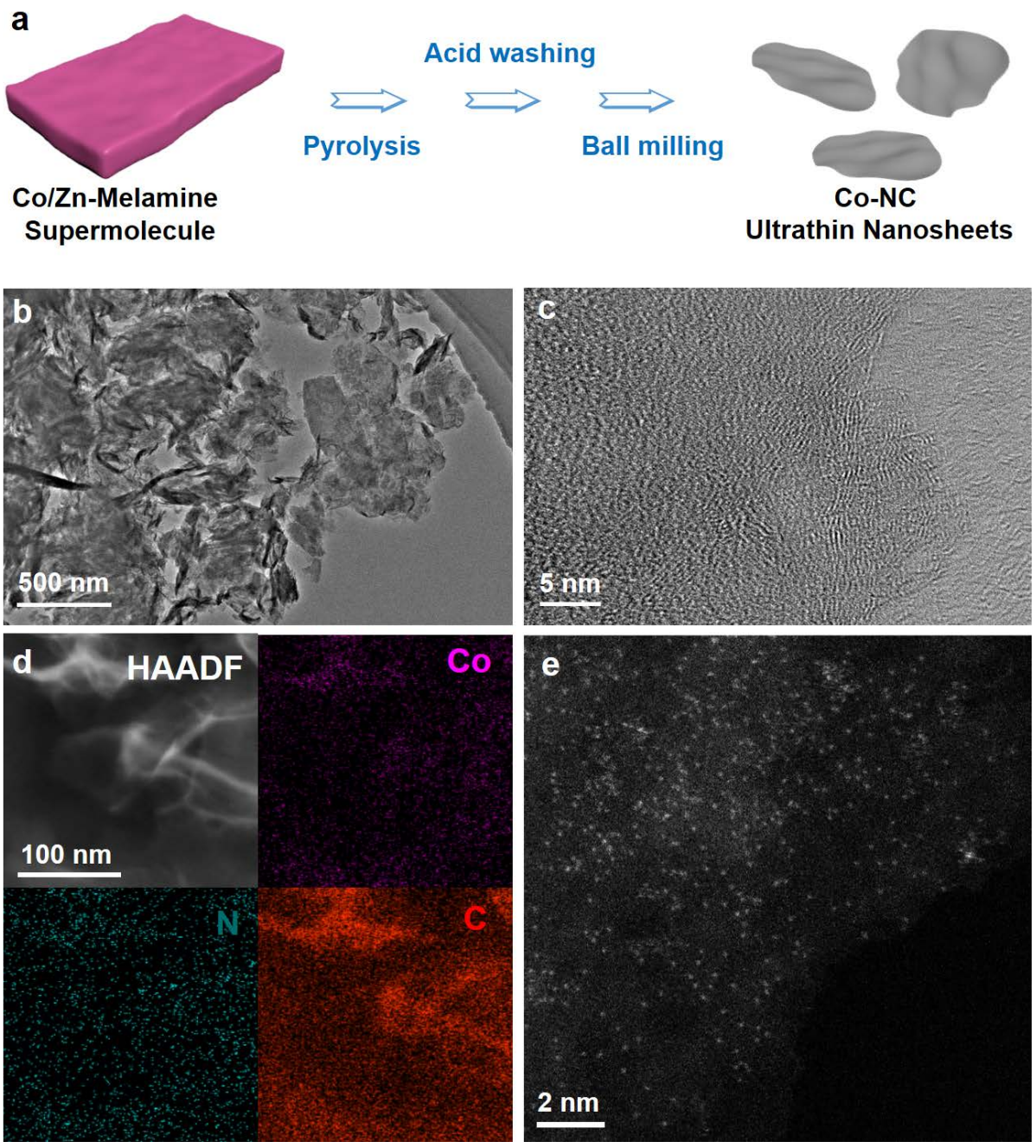

Figure 1. Synthesis and characterizations of Co-NC co-catalyst. (a) Scheme of the formation process. (b, c) TEM images. (d) EDS elemental mapping. (e) Aberration-corrected HAADF-STEM image.

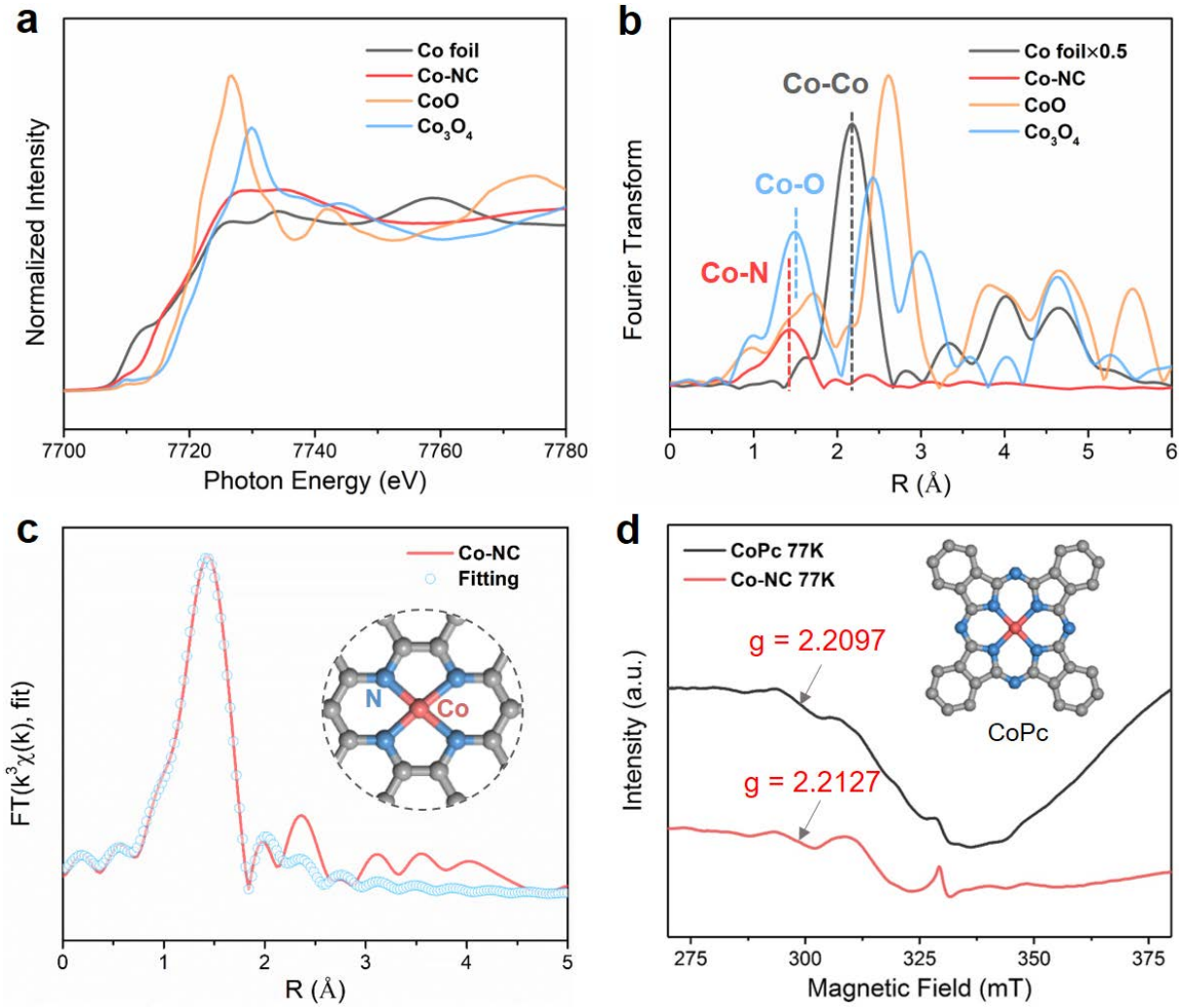

Figure 2. Site coordination analyses of Co-NC co-catalyst. (a) Co K-edge XANES spectra of Co-NC and reference samples. (b) Fourier transformed k^3-weighted χ(k)-function of the EXAFS spectra for Co K-edge. (c) Corresponding EXAFS fitting curve for Co-NC. Inset: the proposed Co-N_4 configuration. (d) ESR spectra of Co-NC and reference CoPc.

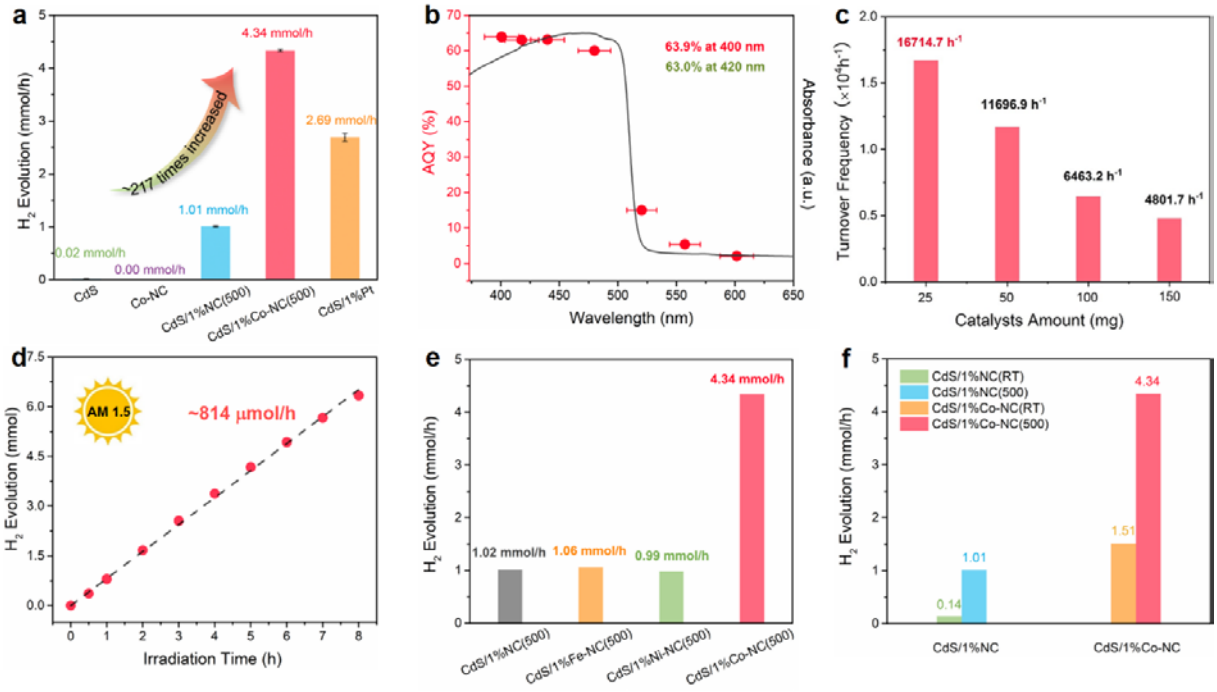

Figure 3. Photocatalytic performance of CdS/Co-NC(500) and reference samples. (a) A comparison of H_2 evolution activity of as-prepared samples. (b) Wavelength-dependent apparent quantum yield (AQY) of H_2 generation from CdS/1%Co-NC(500). (c) Turnover frequency (TOF) calculated based on the single Co sites in CdS/Co-NC(500). (d) H_2 evolution activity of CdS/1%Co-NC(500) under the irradiation of AM 1.5 with a light intensity of 100 mW cm^{-2}. (e) Comparison of H_2 evolution activity over CdS coupled with different co-catalysts (M)-NC (M = Fe, Ni and Co). (f) Comparison of H_2 generation activity of as-prepared samples with and without annealing.

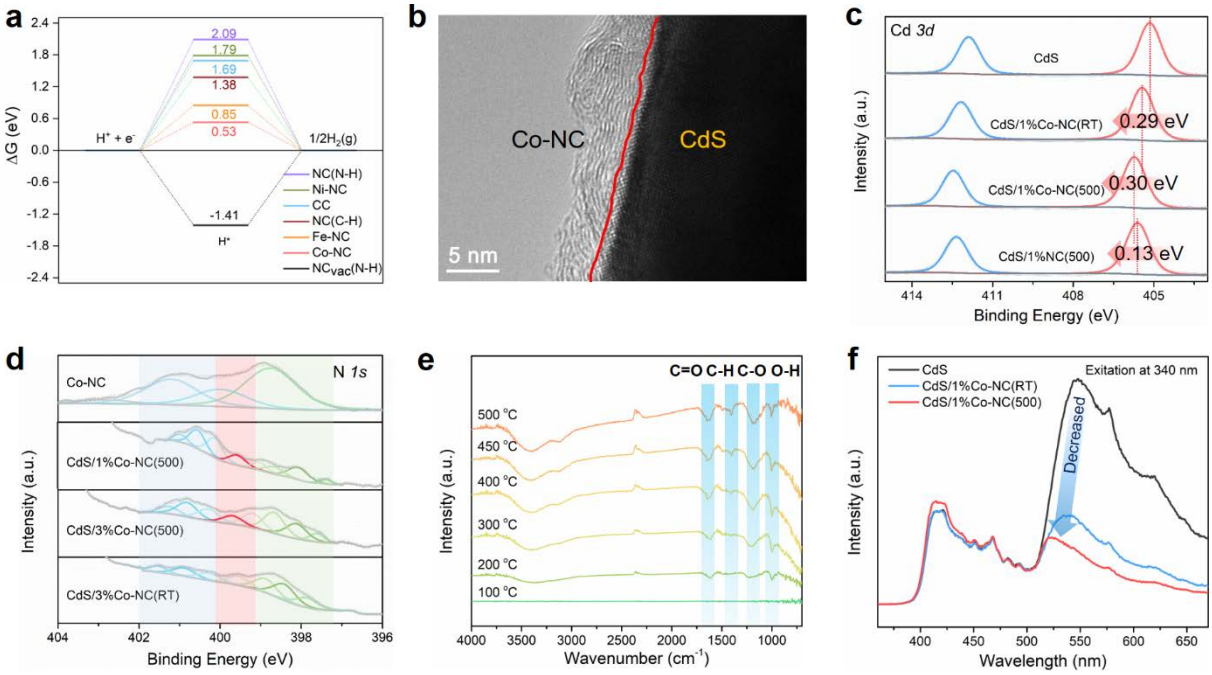

Figure 4. Calculation of isolated Co sites for hydrogen adsorption and characterizations of the relatively clean interface and their promotional effects in charge transport. (a) Calculated Gibbs free energy diagram for hydrogen adsorption on various sites. (b) High resolution TEM image of the interface between CdS and ultrathin Co-NC. (c,d) Cd *3d* and N *1s* XPS spectra of samples. (e) In situ FT-IR spectra of CdS/Co-NC measured at increased temperature. (f) Steady-state photoluminescence spectroscopy of the samples.

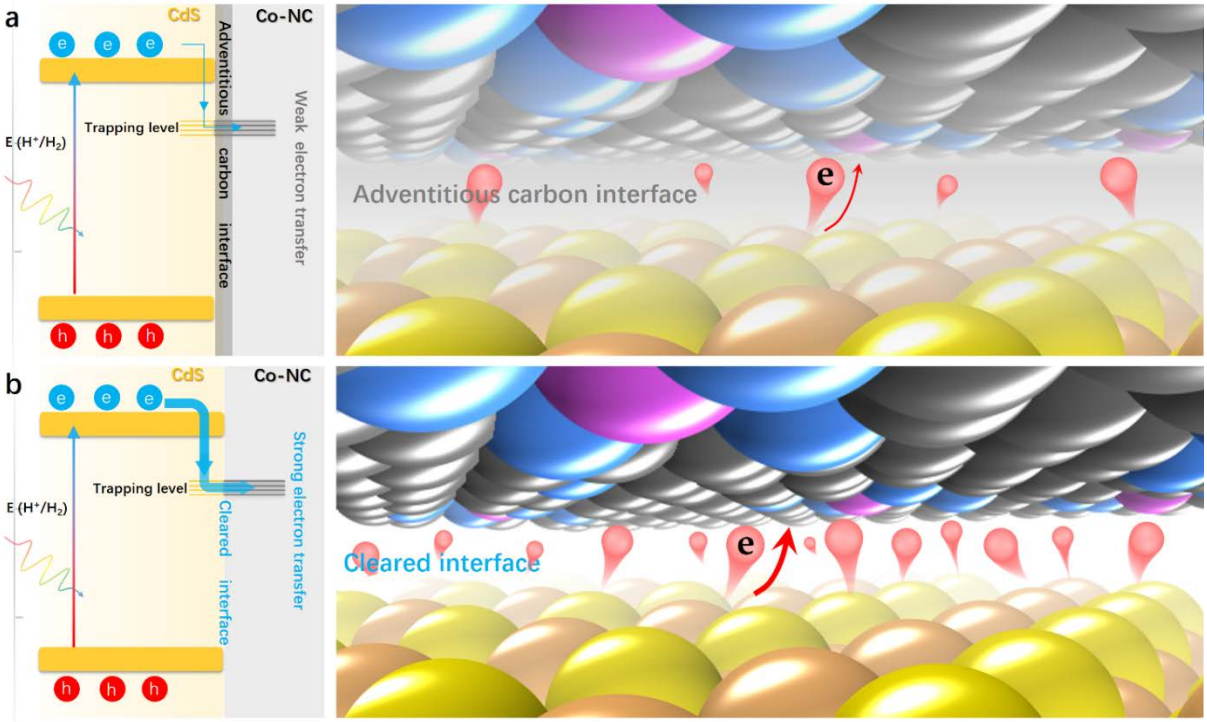

Scheme 1. Origin and mechanism of the efficient photocatalytic system CdS/Co-NC. (a) Illustration of carriers separation and transfer in CdS/Co-NC(RT) system with interfacial adventitious carbon. (b) Scheme of fast electron separation and transfer across cleared interface created by facile calcination treatment for CdS/Co-NC(500).